Numerical vs. Anatomical Variability: Impact on Numerical Reliability on MRI measures of Parkinson's Disease

Yohan Chatelain, Andrzej Sokołowski, Madeleine Sharp, Jean-Baptiste Poline, Tristan Glatard

July 4, 2025

Abstract

Reproducibility in neuroimaging is critically hampered by computational variability within analysis software. Here, we quantify the numerical instability of FreeSurfer, a ubiquitous tool, using structural MRI data from the Parkinson's Progression Markers Initiative. By introducing controlled perturbations with Monte Carlo Arithmetic, we assessed the variability of cortical and subcortical measurements. We found that numerical variability in FreeSurfer is substantial, with key structural metrics often precise to only a single significant digit. This computational noise was frequently comparable to or greater than the biological variation between Parkinson's disease patients and healthy controls. Consequently, the statistical significance of group differences and correlations with clinical severity fluctuated dramatically across identical analyses. Our results demonstrate that subtle computational errors can produce unreliable findings in clinical neuroimaging. Addressing such numerical instability is essential for developing robust biomarkers for neurological disorders like Parkinson's disease.

1 Introduction

Neuroimaging reproducibility has emerged as a critical challenge in neuroscience research. While inter-software variability is well-documented [**?**, **?**, **?**], within-version numerical variability—small output variations from identical software runs—remains underexplored despite potentially significant clinical implications. Numerical variability arises from computational factors including floating-point precision, parallel processing, and random initializations. In Parkinson's disease (PD) research, where MRI-derived metrics like cortical thickness and subcortical volumes serve as potential biomarkers, such variability could obscure subtle disease-related changes and compromise statistical reliability.

Previous studies have demonstrated substantial between-version differences in FreeSurfer outputs [**?**], but the impact of computational uncertainty within single software versions on clinical associations remains unclear. This gap is particularly concerning for PD research, where establishing reliable brain-behavior relationships is essential for developing neuroimaging biomarkers. Despite promising associations between MRI-derived metrics and PD severity, no neuroimaging biomarkers are widely accepted for clinical diagnosis or monitoring. Measurement variability across studies undermines reliability and generalizability, hindering translation to clinical practice. This computational uncertainty could significantly impact PD research by: (1) masking subtle disease-related changes essential for early detection, (2) compromising statistical power for detecting group differences and clinical correlations, and (3) reducing reproducibility across studies using identical analysis pipelines.

Here, we investigate numerical variability in FreeSurfer 7.3.1 using Monte Carlo Arithmetic to simulate realistic computational perturbations. We introduce the Numerical-Anatomical Variability Ratio (ν_{nav}) to quantify computational uncertainty relative to biological variation and derive its theoretical relationship to statistical effect sizes. Using longitudinal data from the Parkinson's Progression Markers Initiative, we assess how numerical precision affects group comparisons and clinical correlations in PD research. Specifically, our aims include: (1) quantifying how computational uncertainty affects group difference detection between PD patients and healthy controls, (2) assessing numerical variability effects on brain-behavior correlations with clinical measures (UPDRS scores), and (3) developing the ν_{nav} framework to predict statistical reliability from computational precision. Our findings will inform strategies for mitigating numerical variability effects and enhancing reproducibility in clinical neuroimaging studies.

2 Results

PD and HC groups showed no significant age differences ($p > 0.05$) but differed in education ($t = -2.05$, $p = 0.04$) and sex distribution ($\chi^2 = 4.15$, $p = 0.04$). The longitudinal cohort showed no significant demographic differences between groups (Table **??**).

2.1 Numerical variability impacts MRI derived findings

We assessed numerical variability in FreeSurfer 7.3.1 using Monte Carlo Arithmetic (MCA) [**?**], more particularly the Fuzzy-libm extension [**?**] that applies random perturbations to mathematical library functions's output. We executed 26 `recon-all` runs for each subject's MRI data, simulating 26 numerical states. Using `recon-all` we collected cortical thickness, surface area, and subcortical volumes for each subject. We present results cortical thickness and subcortical volumes, surface area and cortical volume are reported in the appendix. We selected 103 healthy controls (HC) and 121 Parkinson's disease (PD) patients from the Parkinson's Progression Markers Initiative (PPMI) database.

We tested the statistical significance of group differences and correlations with clinical measures (UPDRS scores) across the 26 MCA repetitions. We reported the fraction of statistically significant tests ($p < 0.05$) for each metric and region. Statistical significance proportions varied substantially for cortical thickness (Figure **??**) and subcortical volumes (Figure **??**). Ratios near 0.5 indicated maximal uncertainty, while values approaching 0 or 1 suggested consistent results across computational variations.

This variability reflects in the partial correlation coefficients and F-statistics from ANCOVA analyses, which showed substantial spread around unperturbed IEEE-754 results used as reference (red markers). This indicates that numerical variability affects both statistical significance and effect size estimation. We note that IEEE results are most of the time included in the distribution of coefficients YC: assert with t-test? but not necessarily at the center of the distribution. We note that the spread of coefficients varies between regions but stay within the same order of magnitude, but some regions show a large spread of coefficients across MCA repetitions.

2.2 ν_{nav} reveals region-specific numerical instabilities

A common issue with neuroimaging analysis is the difficulty in assessing numerical precision and its impact on downstream statistical tests like effect sizes. To address this, we introduce the Numerical-Anatomical Variability Ratio (ν_{nav}), a metric designed to quantify the relationship between numerical variability and anatomical variability, computed as the ratio between the standard deviation of numerical variability and the standard deviation of anatomical variability.

$$\nu_{\text{nav}} = \frac{\sigma_{\text{num}}}{\sigma_{\text{anat}}}$$

Figures **??** and **??** present the ν_{nav} for cortical thickness and subcortical volumes across all brain regions. Regions with high ν_{nav} values indicate areas where numerical variability may compromise the detection of true anatomical differences.

One common measure used in clinical neuroimaging studies is the Cohen's d coefficient that quantifies the effect size of group differences. The ν_{nav} can be used to predict the uncertainty in Cohen's d due to numerical variability. The theoretical relationship between ν_{nav} and Cohen's d uncertainty is given by:

$$\sigma_d = \frac{2}{\sqrt{N}}\nu_{\text{nav}}$$

where σ_d is the standard deviation of Cohen's d and N is the population sample size. We showed in section **??** that this relationship holds true for our data, allowing us to quantify the impact of numerical variability on effect size estimation.

The strength of this relationship is that one can then predict the uncertainty in effect size estimation based on the ν_{nav} value and thus threshold the Cohen's d value based on the ν_{nav} value. Hence, given a paper with Cohen's d values, we can remove values $|\sigma_d| \leq \frac{2}{\sqrt{N}}\nu_{\text{nav}}$ as they will be lower than the numerical variability threshold. This allows us to assess the reliability of the reported effect sizes in the paper. The advantage of this approach is that it can be applied to any neuroimaging study, regardless

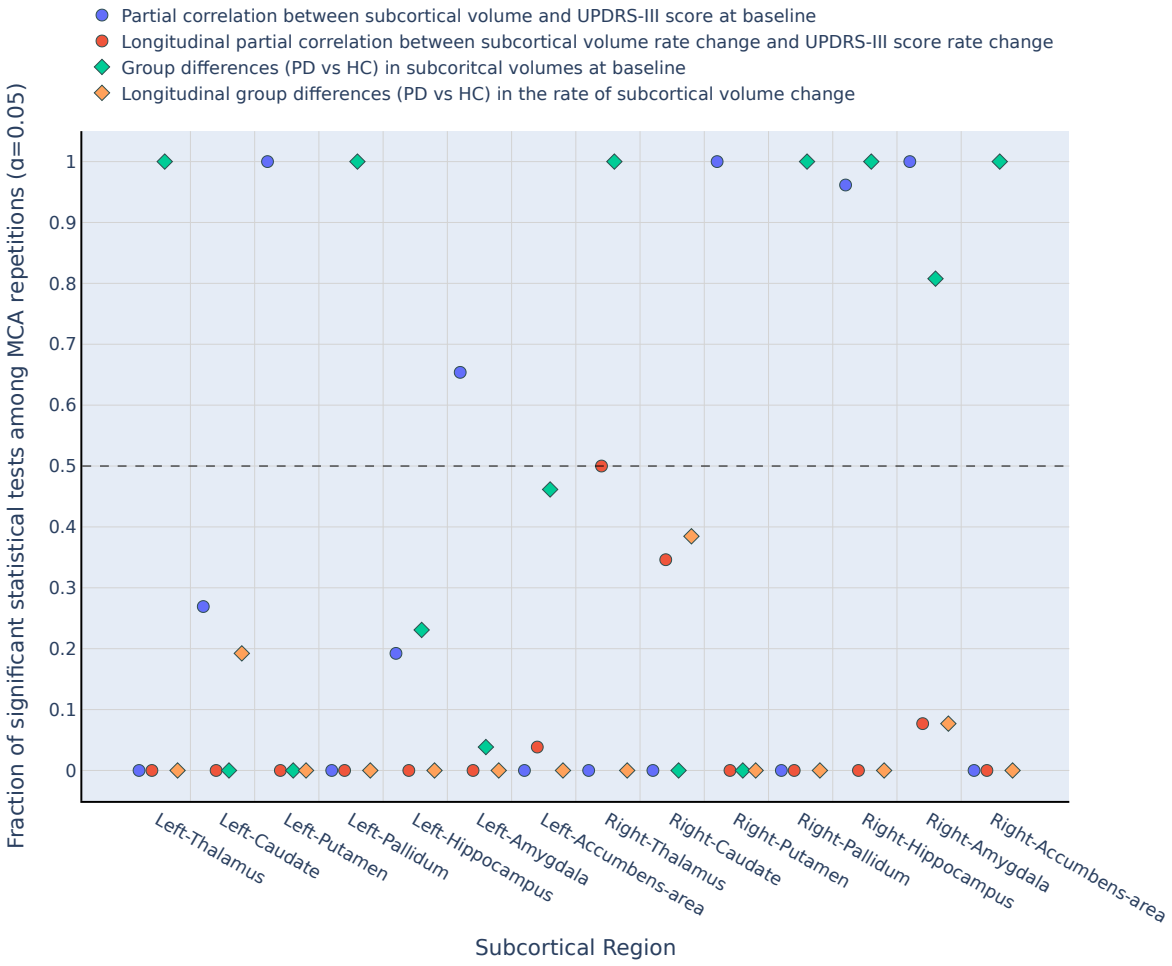

Figure 1: Proportion of statistically significant tests ($p < 0.05$) across the 26 numerical states for subcortical volume measures.

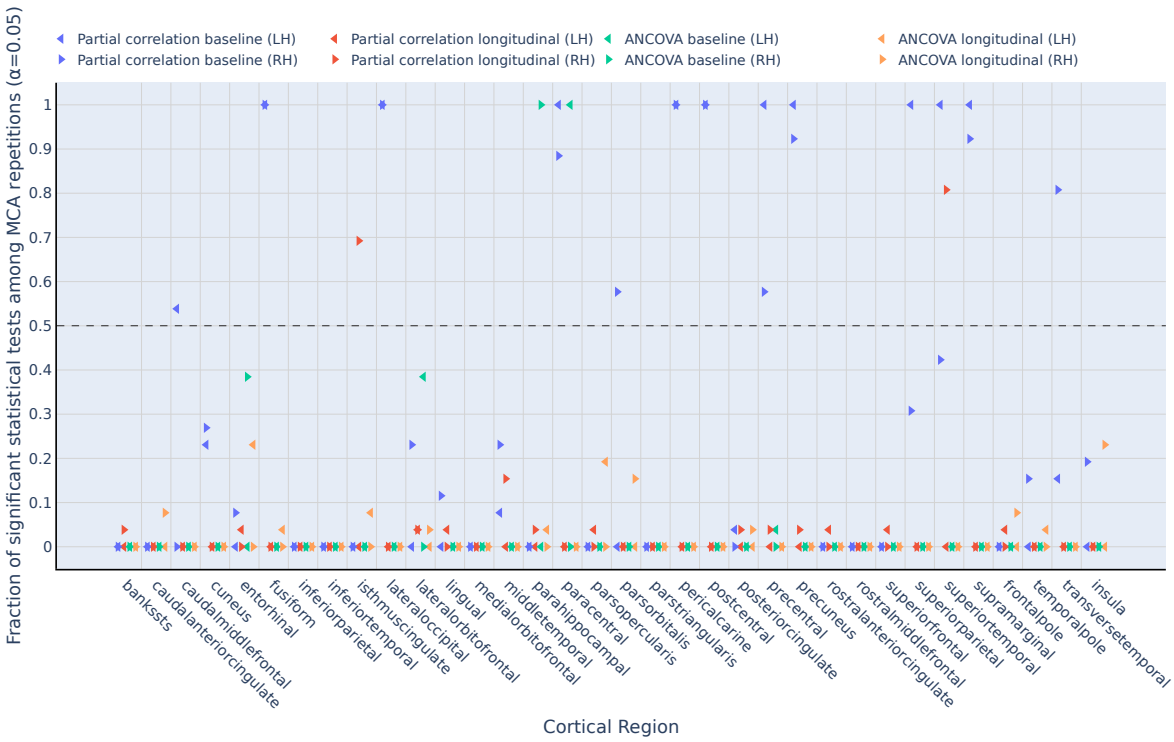

Figure 2: Proportion of statistically significant tests ($p < 0.05$) across the 26 numerical states for cortical thickness measures.

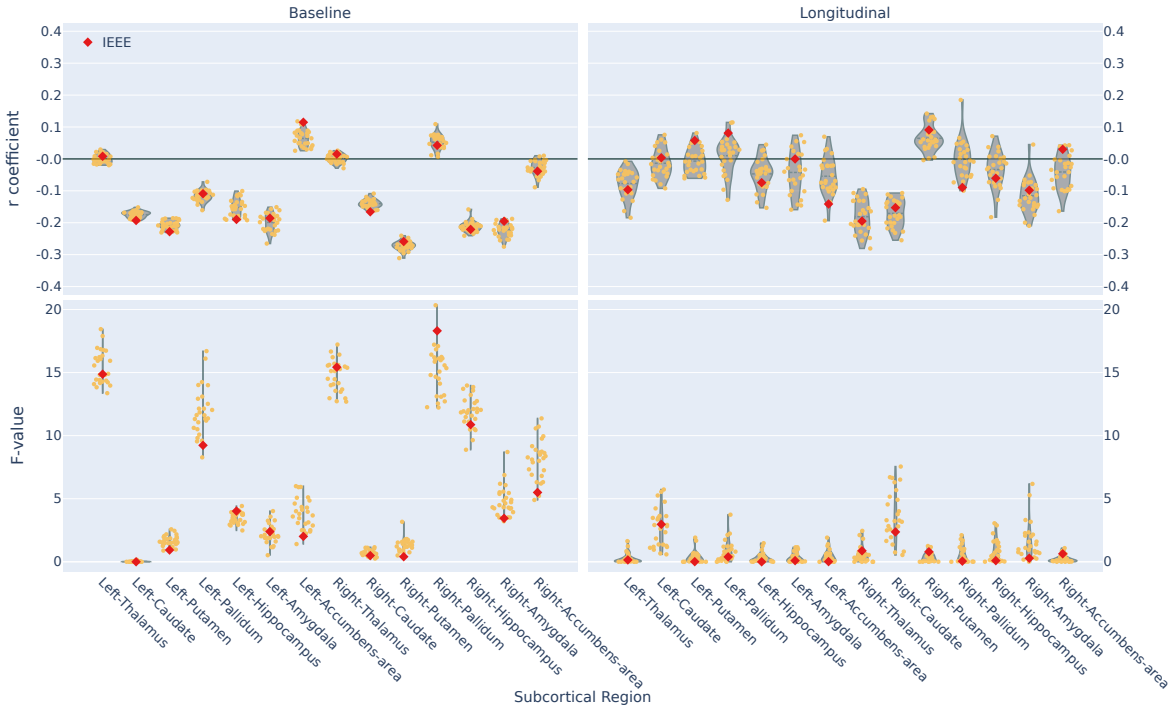

Figure 3: Distribution of partial correlation coefficients (r-values) and F-statistics from ANCOVA across MCA repetitions for subcortical volume measures. Red dots represent the IEEE results. The top row shows r-values, while the bottom row shows F-values. The left column represents baseline analysis, and the right column represents longitudinal analysis.

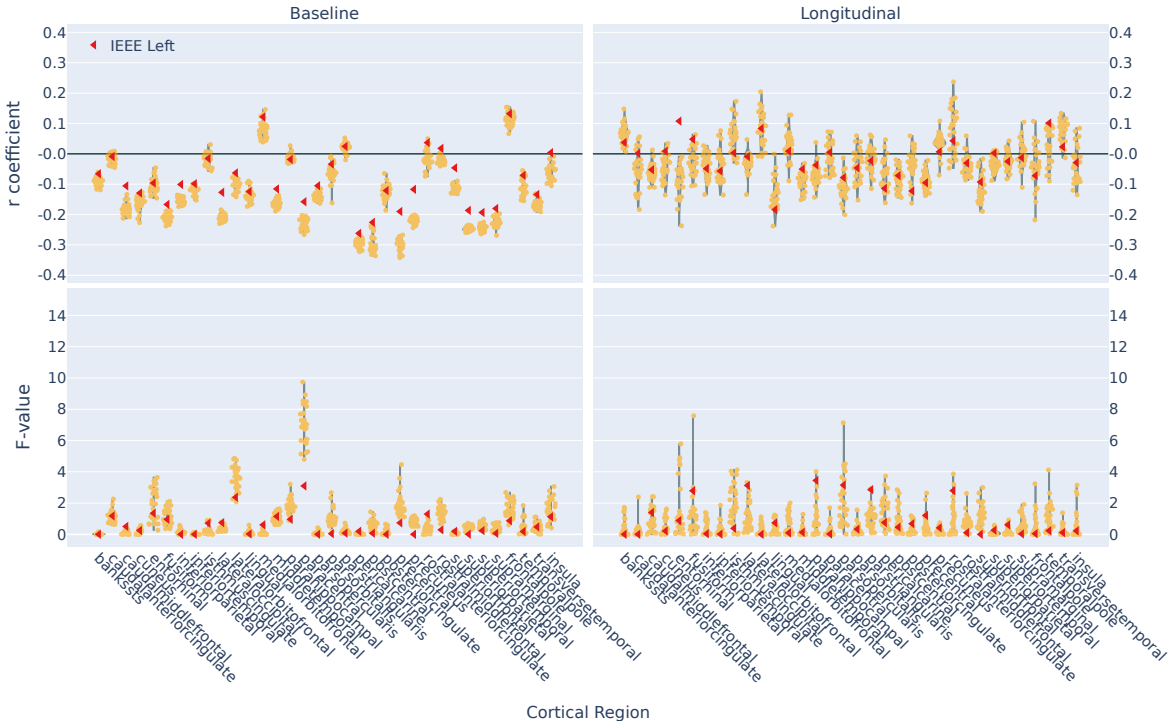

(a) Left hemisphere

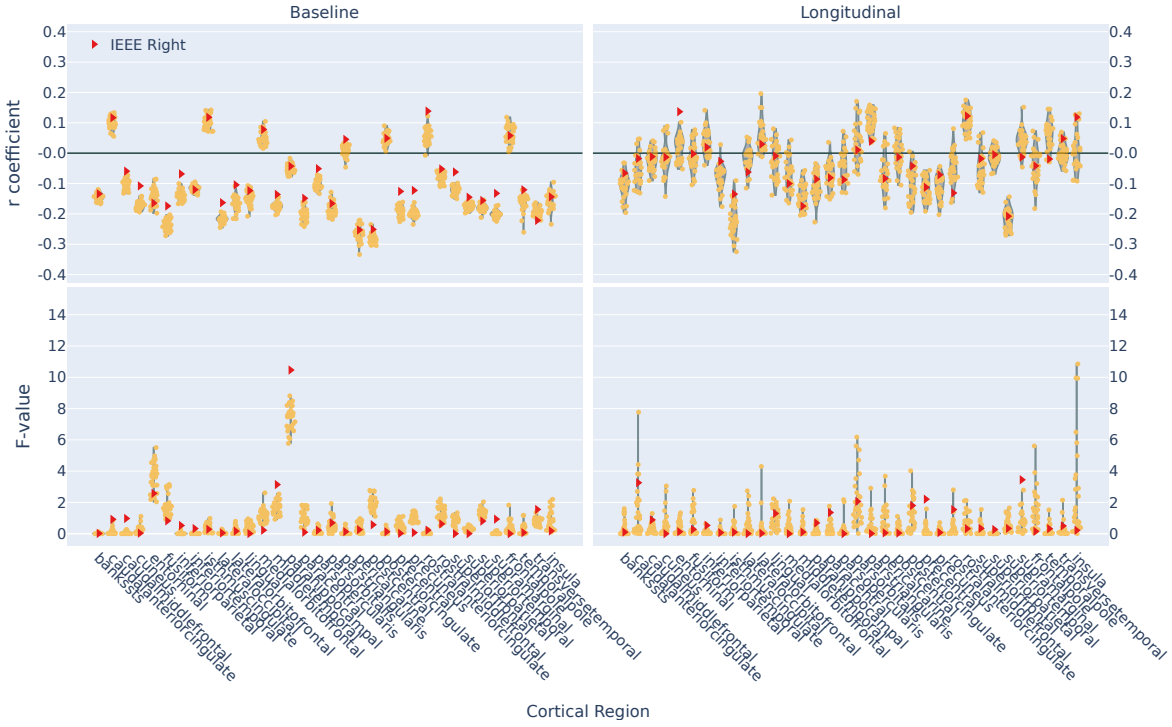

(b) Right hemisphere

Figure 4: Distribution of partial correlation coefficients for cortical thickness across all subjects and regions. Red triangles indicate the IEEE-754 run for reference. The distribution shows the variability in the coefficients, with some regions exhibiting higher consistency than others.

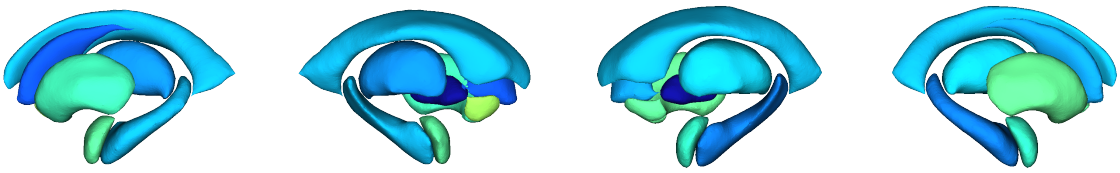

Figure 5: Numerical-Anatomical Variability Ratio (ν_{nav}) for subcortical volumes across regions and groups. Higher ν_{nav} values indicate greater computational uncertainty relative to biological variation.

of the software used, and has a specific value per region, which allows for a more fine-grained analysis of the numerical variability impact on effect size estimation.

The formula also gives a practical way to design experimental studies to ensure a reliable effect size estimation. Figure **??** shows the relationship between ν_{nav} and population sample size N for predicting the uncertainty in Cohen's d effect size estimation σ_d. The contour lines represent different σ_d order of magnitude, showing how numerical variability scales with sample size. User can hence refers to this to select the sample size N to ensure a reliable effect size estimation. For example, with a typical ν_{nav} value of 0.2, to maintain reliable effect size estimates $\sigma_d \leq 0.01$, the plot suggests to use $N \geq 1500$. This provides a practical guideline for researchers to ensure that their sample size is large enough to obtain reliable effect size estimates, taking into account the numerical variability introduced by the analysis software.

2.3 ν_{nav} helps thresholding effect size uncertainty

We applied the ν_{nav} framework to assess the reliability of reported effect on ENIGMA studies [**?**]. We extracted the Cohen's d using the `enigmatoolbox` Python package [**?**] colored in black regions where the Cohen's d is below the numerical variability threshold. Figure **??** shows the results of this analysis.

3 Discussion

Our analysis reveals significant numerical instability in FreeSurfer 7.3.1, with cortical measurements showing limited precision (1-1.5 significant digits) that substantially impacts statistical reliability in neuroimaging studies. These precision limitations pose particular challenges for detecting subtle disease-related changes in conditions like Parkinson's disease.

The absence of significant baseline differences between PD and HC groups, combined with inconsistent cluster detection (only 1/26 clusters reproduced across repetitions), demonstrates how numerical variability can compromise reproducibility. The ν_{nav} framework quantifies this relationship, showing that computational uncertainty approaches or exceeds biological variation in many brain regions.

Statistical test consistency varied markedly across MCA repetitions, with methodological choices (Z-test vs. permutation test) further influencing outcome reliability. Effect size distributions showed substantial spread around standard IEEE-754 results, indicating that numerical precision directly affects both significance testing and effect size estimation.

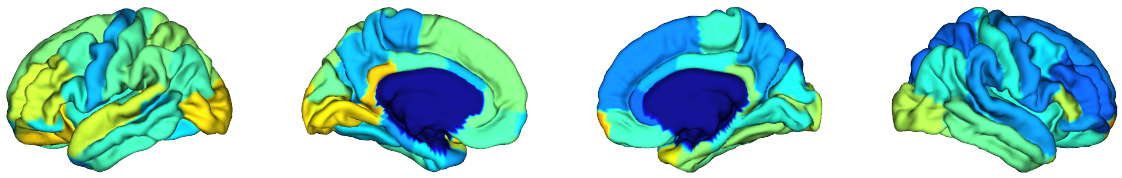

Figure 6: Numerical-Anatomical Variability Ratio (ν_{nav}) for cortical thickness across regions and groups. Higher ν_{nav} values indicate greater computational uncertainty relative to biological variation. The color scale indicates the ν_{nav} value, with warmer colors indicating higher ν_{nav} values.

Importantly, inter-subject variability exceeded intra-subject variability, suggesting that FreeSurfer maintains relative consistency across different individuals despite numerical limitations. This supports continued use while highlighting the need for improved computational precision in future neuroimaging software development. This study demonstrates significant numerical limitations in FreeSurfer 7.3.1, with cortical measurements exhibiting only 1-1.5 significant digits of precision. These computational constraints substantially impact statistical reliability and reproducibility in neuroimaging research, particularly for detecting subtle disease-related changes.

Our ν_{nav} framework quantifies the relationship between computational uncertainty and biological variation, revealing that numerical instability approaches or exceeds anatomical variability in many brain regions. This finding has direct implications for statistical power, as demonstrated by inconsistent cluster detection (only 1/26 clusters reproduced) and variable effect sizes across identical analyses.

While inter-subject variability exceeded intra-subject variability—supporting relative consistency across individuals—the absence of significant PD-HC differences and weak clinical correlations highlight how numerical limitations can mask true biological signals. The theoretical relationship between ν_{nav} and Cohen's d uncertainty provides a framework for predicting statistical reliability based on computational precision.

These findings emphasize the critical need for improved numerical precision in neuroimaging software. Future developments should prioritize computational stability to enhance the detection of subtle neurological changes and improve reproducibility across studies. The ν_{nav} framework offers a practical tool for assessing and comparing the numerical reliability of neuroimaging methodologies.

4 Methods

4.1 Numerical variability assessment

We employed Monte Carlo Arithmetic (MCA) [**?**] to quantify numerical instability in FreeSurfer computations. MCA introduces controlled random perturbations into floating-point operations, simulating rounding errors that occur across different computational environments. This stochastic approach enables systematic assessment of result stability by measuring variation across multiple runs of identical analyses.

We used Fuzzy-libm [**?**], which extends MCA to mathematical library functions (`exp`, `log`, `sin`, `cos`) through Verificarlo [**?**], an LLVM-based compiler. Virtual precision parameters were set to 53

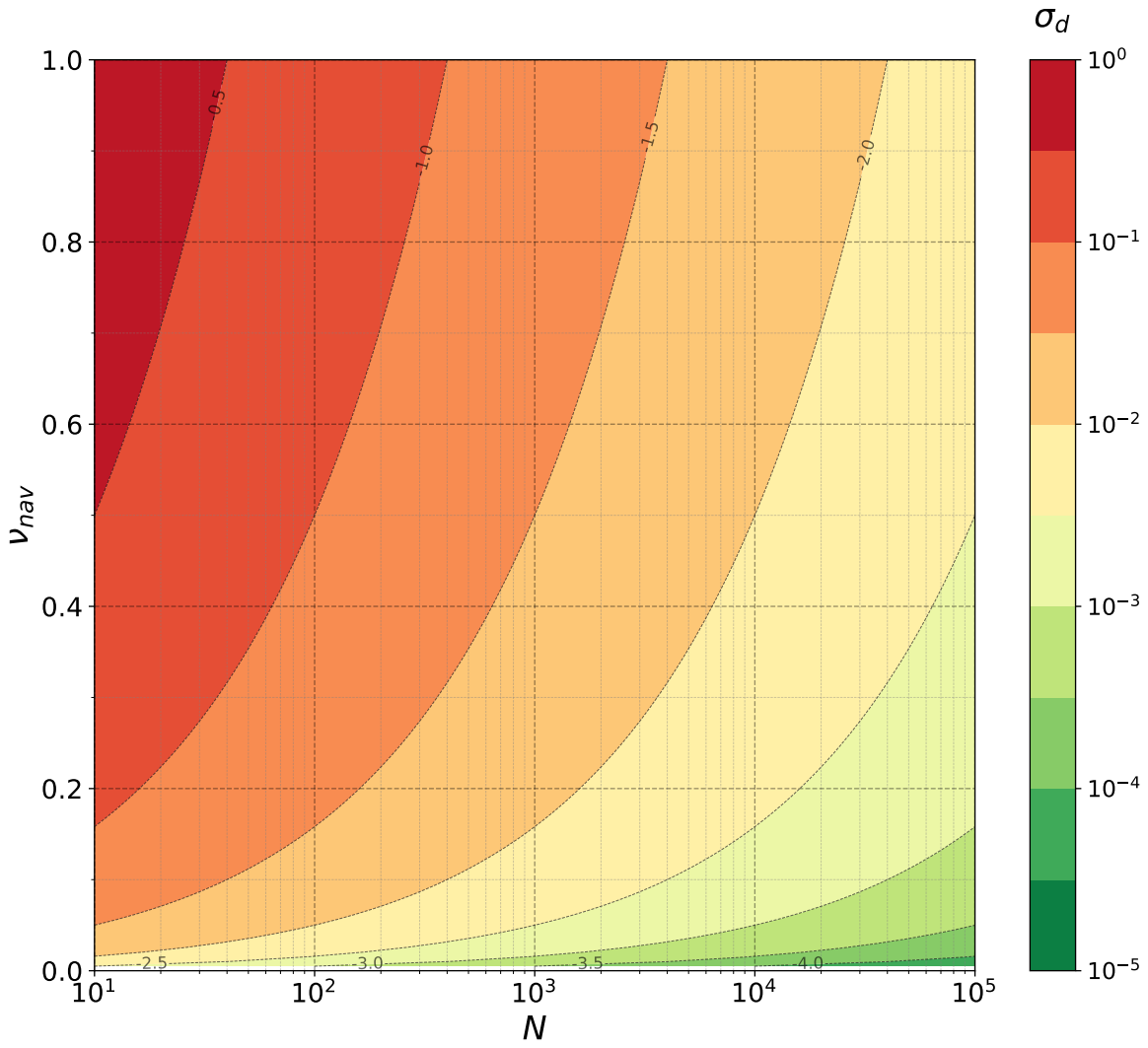

Figure 7: Relationship between ν_{nav} and population sample size N for predicting the uncertainty in Cohen's d effect size estimation σ_d. The contour lines represent different ν_{nav} values, showing how numerical variability scales with sample size. With a typical ν_{nav} value of 0.2, to maintain reliable effect size estimates $\sigma_d \leq 0.01$, the plot suggests to use $N \geq 1500$.

bits for double precision and 24 bits for single precision to simulate realistic machine-level precision errors.

4.2 Participants

We analyzed data from the Parkinson's Progression Markers Initiative (PPMI), a multi-site longitudinal study. From 316 initial participants, we selected 125 Parkinson's disease patients without mild cognitive impairment (PD-non-MCI) and 106 healthy controls (HC) with complete longitudinal T1-weighted MRI data. PD-MCI patients were excluded to avoid confounding effects of cognitive impairment.

Inclusion criteria required: (1) primary PD diagnosis or healthy control status, (2) availability of two visits with T1-weighted scans, and (3) absence of other neurological diagnoses. PD severity was assessed using the Unified Parkinson's Disease Rating Scale (UPDRS). The study received ethics approval from participating institutions, and all participants provided written informed consent (Table **??**).

Cohort	**HC**	**PD-non-MCI**
n	103	121
Age (y)	60.7 ± 10.3	60.7 ± 9.1
Age range	$30.6 - 84.3$	$39.2 - 78.3$
Gender (male, %)	57 (55.3%)	80 (66.1%)
Education (y)	16.6 ± 3.3	16.1 ± 3.0
UPDRS III OFF baseline	–	23.4 ± 10.1
UPDRS III OFF follow-up	–	25.8 ± 11.1
Duration T2 - T1 (y)	1.4 ± 0.5	1.4 ± 0.7

Table 1: **Abbreviations:** MCI = Mild Cognitive Impairment; UPDRS = Unified Parkinson's Disease Rating Scale; PD = Parkinson's disease. Values are expressed as mean ± standard deviation. PD-non-MCI longitudinal sample is a subsample of the PD-non-MCI original sample that had longitudinal data and disease severity scores available.

4.3 Image acquisition and preprocessing

T1-weighted MRI images were obtained from PPMI that uses standardized acquisition parameters: repetition time = 2.3 s, echo time = 2.98 s, inversion time = 0.9 s, slice thickness = 1 mm, number of slices = 192, field of view = 256 mm, and matrix size = 256×256. However, since PPMI is a multisite project there may be slight differences in the sites' setup.

We processed images using FreeSurfer 7.3.1 instrumented with Fuzzy-libm to introduce controlled numerical perturbations. Each participant underwent 34 `recon-all` executions, extracting cortical thickness, surface area, and volumes. After quality control and exclusion of failed runs, we randomly selected 26 successful repetitions per subject to ensure balanced datasets for statistical analysis.

Longitudinal processing followed the standard FreeSurfer stream [**?**]: cross-sectional processing of both timepoints, followed by creation of an unbiased within-subject template [**?**] using robust registration [**?**]. Downstream analyses used unperturbed FreeSurfer to prevent additional numerical perturbations.

4.4 Numerical Variability Assessment

We assessed FreeSurfer 7.3.1 numerical stability in cross-sectional and longitudinal contexts using the Numerical-Anatomical Variability Ratio (ν_{nav}) and its relationship to statistical effect sizes.

4.4.1 Numerical-Anatomical Variability Ratio (ν_{nav})

To quantify computational stability relative to biological variation, we developed the Numerical-Anatomical Variability Ratio (ν_{nav}). For each brain region, ν_{nav} measures the ratio of measurement uncertainty arising from computational processes to natural inter-subject anatomical variation:

$$\nu_{\text{nav}} = \frac{\sigma_{\text{num}}}{\sigma_{\text{anat}}}$$

where σ_{num} represents numerical variability (measurement precision across MCA repetitions for individual subjects) and σ_{anat} represents anatomical variability (inter-subject differences within each repetition).

For each region of interest, measurements from n MCA repetitions across m subject-visit pairs form a data matrix $\mathcal{M}_{n\times m}$, where element $x_{i,j}$ represents the measurement for subject j in repetition i.

Numerical variability quantifies intra-subject measurement consistency:

$$\sigma^2_{\text{num}} = \frac{1}{m}\sum_{j=1}^{m}\left[\frac{1}{n-1}\sum_{i=1}^{n}(x_{i,j} - \bar{x}_{\cdot,j})^2\right] \tag{1}$$

Anatomical variability captures inter-subject differences:

$$\sigma^2_{\text{anat}} = \frac{1}{n}\sum_{i=1}^{n}\left[\frac{1}{m-1}\sum_{j=1}^{m}(x_{i,j} - \bar{x}_{i,\cdot})^2\right] \tag{2}$$

where $\bar{x}_{\cdot,j}$ and $\bar{x}_{i,\cdot}$ denote column and row means, respectively. Higher ν_{nav} values indicate regions where computational uncertainty approaches or exceeds biological variation, potentially compromising the detection of true anatomical differences.

4.4.2 Relationship between ν_{nav} and Effect Size Uncertainty

We derived the theoretical relationship between ν_{nav} and Cohen's d variability to quantify how measurement uncertainty affects statistical effect sizes in group comparisons.

For a balanced two-group design with total sample size N, each observation decomposes as $X_{ij} = \mu_i + \varepsilon_{ij}^{(\text{anat})} + \varepsilon_{ij}^{(\text{num})}$, where μ_i represents the true group mean, $\varepsilon_{ij}^{(\text{anat})} \sim \mathcal{N}(0, \sigma^2_{\text{anat}})$ captures anatomical variation, and $\varepsilon_{ij}^{(\text{num})} \sim \mathcal{N}(0, \sigma^2_{\text{num}})$ represents numerical uncertainty.

The standard deviation of Cohen's d attributable to measurement error is:

$$\sigma_d = \frac{2}{\sqrt{N}} \cdot \nu_{\text{nav}} \tag{3}$$

This relationship emerges from error propagation analysis. The difference in group means has variance $\text{Var}(\bar{X}_1 - \bar{X}_2) = 4(\sigma^2_{\text{anat}} + \sigma^2_{\text{num}})/N$, with the numerical component contributing $4\sigma^2_{\text{num}}/N$. Since Cohen's d normalizes by the pooled standard deviation $\sqrt{\sigma^2_{\text{anat}} + \sigma^2_{\text{num}}}$, the measurement error contribution becomes $\sigma_d = (2\sigma_{\text{num}}/\sqrt{N})/\sigma_{\text{anat}} = (2/\sqrt{N}) \cdot \nu_{\text{nav}}$.

This formula indicates that regions with $\nu_{\text{nav}} = 0.1$ contribute approximately $0.2/\sqrt{N}$ uncertainty to Cohen's d, while regions with $\nu_{\text{nav}} = 1.0$ contribute $2/\sqrt{N}$ uncertainty. The relationship provides a direct link between computational stability (ν_{nav}) and statistical reliability in neuroimaging studies.

5 Data Availability

The data that support the findings of this study are available from the Parkinson's Progression Markers Initiative (PPMI) database (www.ppmi-info.org/access-data-specimens/download-data), but restrictions apply to the availability of these data, which were used under license for the current study, and so are not publicly available. Data are however available from the authors upon reasonable request and with permission of the PPMI.

6 Code Availability

The code used to conduct the analyses is available at [URL to be added upon publication].

7 Acknowledgements

The analyses were conducted on the Virtual Imaging Platform [**?**], which utilizes resources provided by the Biomed virtual organization within the European Grid Infrastructure (EGI). We extend our gratitude to Sorina Pop from CREATIS, Lyon, France, for her support.

References

[BBD+21] Nikhil Bhagwat, Amadou Barry, Erin W Dickie, Shawn T Brown, Gabriel A Devenyi, Koji Hatano, Elizabeth DuPre, Alain Dagher, Mallar Chakravarty, Celia MT Greenwood, et al. Understanding the impact of preprocessing pipelines on neuroimaging cortical surface analyses. *GigaScience*, 10(1):giaa155, 2021.

[BNHC+20] Rotem Botvinik-Nezer, Felix Holzmeister, Colin F Camerer, Anna Dreber, Juergen Huber, Magnus Johannesson, Michael Kirchler, Roni Iwanir, Jeanette A Mumford, R Alison Adcock, et al. Variability in the analysis of a single neuroimaging dataset by many teams. *Nature*, 582(7810):84–88, 2020.

[DdOCP16] Christophe Denis, Pablo de Oliveira Castro, and Eric Petit. Verificarlo: checking floating point accuracy through monte carlo arithmetic. In *2016 IEEE 23nd Symposium on Computer Arithmetic (ARITH)*, 2016.

[GHJ+12] Ed HBM Gronenschild, Petra Habets, Heidi IL Jacobs, Ron Mengelers, Nico Rozendaal, Jim Van Os, and Machteld Marcelis. The effects of freesurfer version, workstation type, and macintosh operating system version on anatomical volume and cortical thickness measurements. *PloS one*, 7(6):e38234, 2012.

[GLG+12] Tristan Glatard, Carole Lartizien, Bernard Gibaud, Rafael Ferreira Da Silva, Germain Forestier, Frédéric Cervenansky, Martino Alessandrini, Hugues Benoit-Cattin, Olivier Bernard, Sorina Camarasu-Pop, et al. A virtual imaging platform for multi-modality medical image simulation. *IEEE transactions on medical imaging*, 32(1):110–118, 2012.

[HPZ+23] Elizabeth Haddad, Fabrizio Pizzagalli, Alyssa H Zhu, Ravi R Bhatt, Tasfiya Islam, Iyad Ba Gari, Daniel Dixon, Sophia I Thomopoulos, Paul M Thompson, and Neda Jahanshad. Multisite test–retest reliability and compatibility of brain metrics derived from freesurfer versions 7.1, 6.0, and 5.3. *Human Brain Mapping*, 44(4):1515–1532, 2023.

[LPP+21] Sara Larivière, Casey Paquola, Bo-yong Park, Jessica Royer, Yezhou Wang, Oualid Benkarim, Reinder Vos de Wael, Sofie L Valk, Sophia I Thomopoulos, Matthias Kirschner, et al. The enigma toolbox: multiscale neural contextualization of multisite neuroimaging datasets. *Nature Methods*, 18(7):698–700, 2021.

[Par97] Douglass Stott Parker. *Monte Carlo arithmetic: exploiting randomness in floating-point arithmetic*. Citeseer, 1997.

[RF11] Martin Reuter and Bruce Fischl. Avoiding asymmetry-induced bias in longitudinal image processing. *Neuroimage*, 57(1):19–21, 2011.

[RRF10] Martin Reuter, H Diana Rosas, and Bruce Fischl. Highly accurate inverse consistent registration: a robust approach. *Neuroimage*, 53(4):1181–1196, 2010.

[RSRF12] Martin Reuter, Nicholas J Schmansky, H Diana Rosas, and Bruce Fischl. Within-subject template estimation for unbiased longitudinal image analysis. *Neuroimage*, 61(4):1402–1418, 2012.

[SCF+21] Devan Sohier, Pablo De Oliveira Castro, François Févotte, Bruno Lathuilière, Eric Petit, and Olivier Jamond. Confidence intervals for stochastic arithmetic. *ACM Transactions on Mathematical Software (TOMS)*, 47(2):1–33, 2021.

[SCKG21] Ali Salari, Yohan Chatelain, Gregory Kiar, and Tristan Glatard. Accurate simulation of operating system updates in neuroimaging using monte-carlo arithmetic. In *Uncertainty for Safe Utilization of Machine Learning in Medical Imaging, and Perinatal Imaging, Placental and Preterm Image Analysis: 3rd International Workshop, UNSURE 2021, and 6th International Workshop, PIPPI 2021, Held in Conjunction with MICCAI 2021, Strasbourg, France, October 1, 2021, Proceedings 3*, pages 14–23. Springer, 2021.

[TSM+14] Paul M Thompson, Jason L Stein, Sarah E Medland, Derrek P Hibar, Alejandro Arias Vasquez, Miguel E Renteria, Roberto Toro, Neda Jahanshad, Gunter Schumann, Barbara Franke, et al. The enigma consortium: large-scale collaborative analyses of neuroimaging and genetic data. *Brain imaging and behavior*, 8:153–182, 2014.

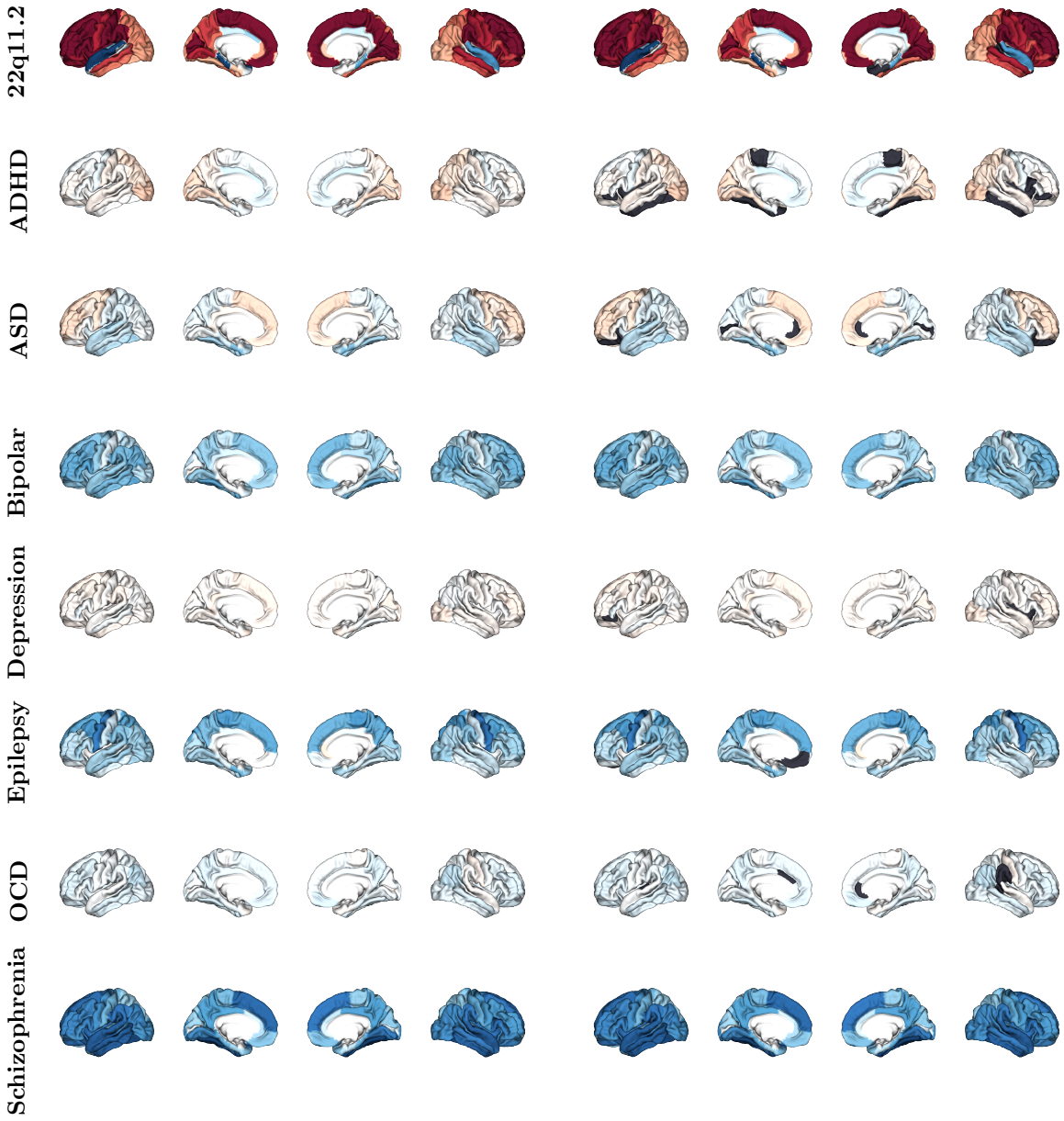

Figure 8: ENIGMA cortical thickness Cohen's d maps showing unthresholded effect sizes (left) and effect sizes thresholded by the ν_{NA} framework (right) for different disorders. Black regions indicate areas where Cohen's d values fall below the numerical variability threshold, demonstrating regions where reported effect sizes may be unreliable due to computational uncertainty.

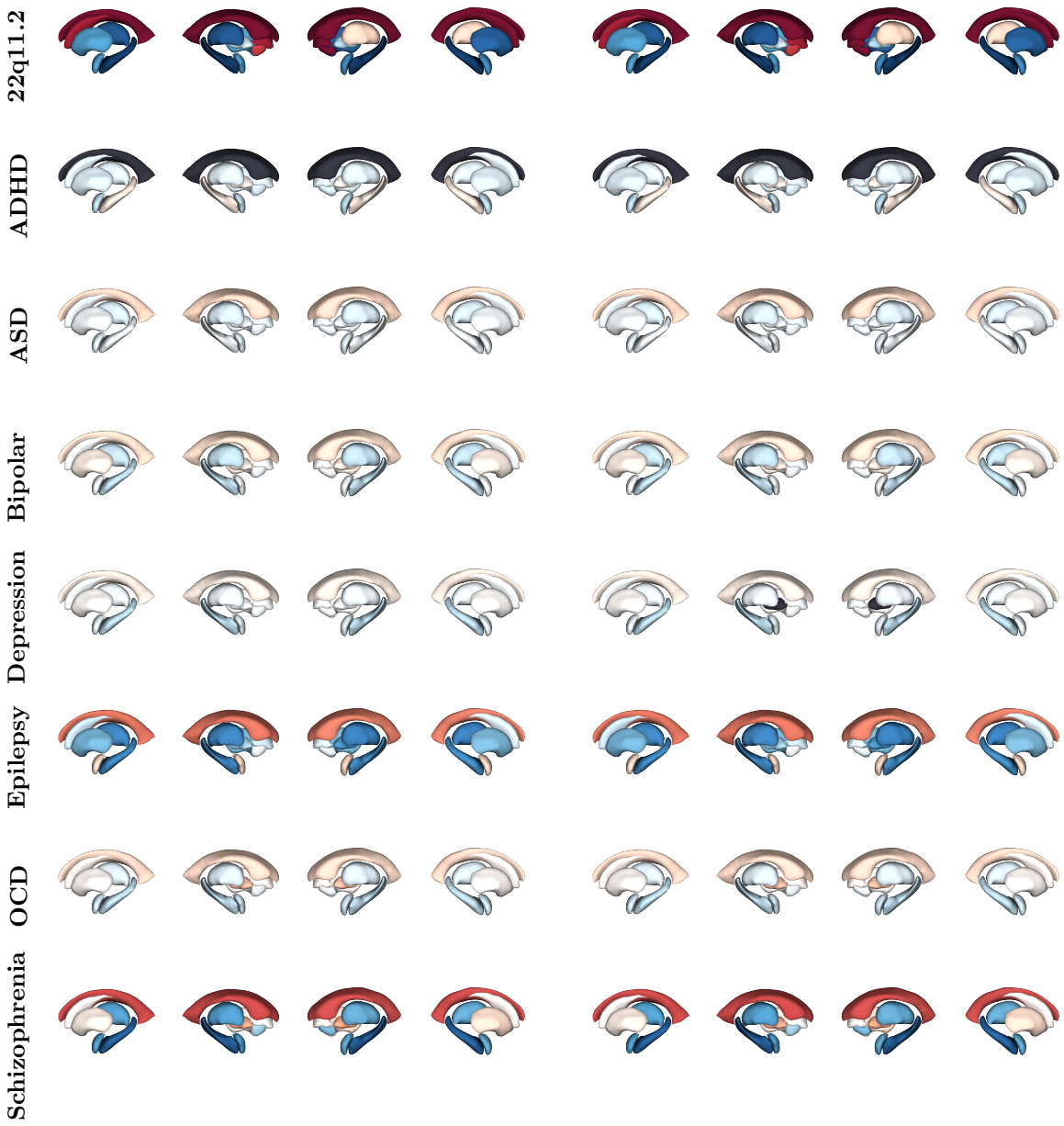

Figure 9: ENIGMA subcortical volume Cohen's d maps showing unthresholded effect sizes (left) and effect sizes thresholded by the ν_{NA} framework (right) for different disorders. Black regions indicate areas where Cohen's d values fall below the numerical variability threshold, demonstrating regions where reported effect sizes may be unreliable due to computational uncertainty.

A Formula

A.1 Significant digits formula

We compute the number of significant bits $\hat{s}$ with probability $p_s = 0.95$ and confidence $1 - \alpha_s = 0.95$ using the `significantdigits` package[1] (version 0.4.0). `significantdigits` implements the Centered Normality Hypothesis approach described in [**?**]:

$$\hat{s_i} = -\log_2 \left| \frac{\hat{\sigma_i}}{\hat{\mu_i}} \right| - \delta(n, \alpha_s, p_s),$$

where $\hat{\sigma_i}$ and $\hat{\mu_i}$ are the average and standard deviation over the repetitions, and

$$\delta(n, \alpha_s, p_s) = \log_2 \left(\sqrt{\frac{n-1}{\chi^2_{1-\alpha_s/2}}} \Phi^{-1} \left(\frac{p_s + 1}{2} \right) \right) \tag{4}$$

is a penalty term for estimating $\hat{s_i}$ with probability p_s and confidence level $1 - \alpha_s$ for a sample size n. Φ^{-1} is the inverse cumulative distribution of the standard normal distribution and χ^2 is the Chi-2 distribution with n-1 degrees of freedom.

A.2 Extended Sørensen-Dice coefficient

The extended Sørensen-Dice coefficient is a measure of overlap between multiple sets, defined as follows:

$$\text{Dice}(A_1, A_2, \ldots, A_n) = \frac{n \left| \bigcap_{i=1}^{n} A_i \right|}{\sum_{i=1}^{n} |A_i|}$$

.

B Cross-sectional Analysis

As a side result, the cross-sectional analysis measures the impact of numerical variability in FreeSurfer version 7.3.1 on the PPMI (Parkinson's Progression Markers Initiative) cohort. This involves comparing the estimation of structural MRI measures, including cortical and subcortical volumes, cortical thickness, and surface area. The goal is to assess the stability of these key metrics and quantify the numerical variability.

FreeSurfer 7.3.1 showed limited numerical precision across all cortical measures: 1.61 ± 0.20 significant digits for cortical thickness, 1.33 ± 0.23 for surface area, and 1.33 ± 0.23 for cortical volume (Figures **??**). Subcortical volumes have a similar precision with 1.33 ± 0.22 significant digits on average (Figure **??**). These values indicate measurements are typically precise to only one decimal place, with some instances showing complete precision loss. Regional consistency was observed within each metric type, with cortical thickness showing the highest precision (range: $1.22 - 1.93$ digits) compared to surface area ($0.82 - 1.72$ digits) and cortical volume ($0.80 - 1.72$ digits). Subcortical volumes exhibited the highest precision (range: $0.88 - 1.57$ digits), with a mean of 1.33 ± 0.22 significant digits.

To measure the structural overlap, we evaluated using the extended Sørensen-Dice coefficient: Dice coefficients revealed substantial inter-subject variability, particularly in temporal pole regions (Figure **??**). We also observed that the Dice coefficient varies across regions, with some regions showing higher variability than others with cortical volume ($0.00 - 0.91$) with a mean of 0.75 ± 0.11 and subcortical volume ($0.18 - 0.94$) with a mean of 0.82 ± 0.08. Finally, we noticed that subcortical volume measurements are more stable than cortical volume.

B.1 Significant digits average across all subjects

[1] https://github.com/verificarlo/significantdigits

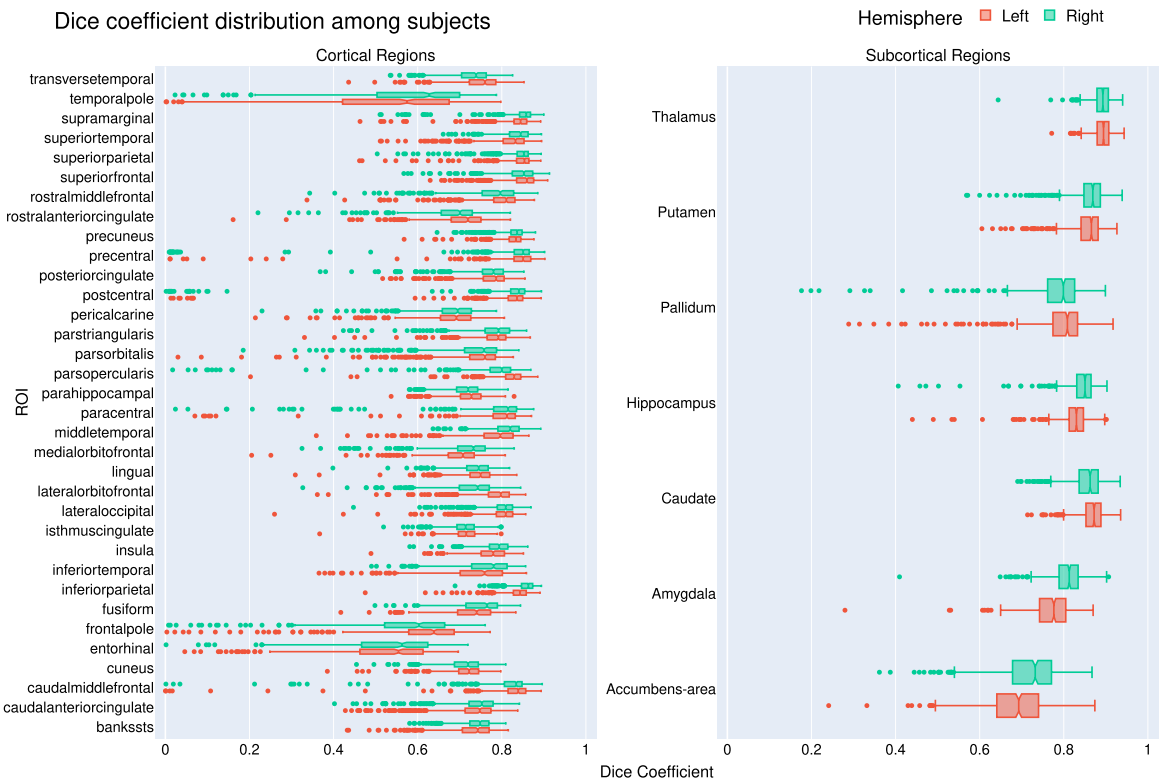

Figure 10: Dice coefficient.

Table 2: Significant digits average across all subjects.

Region	**cortical thickness**		**surface area**		**cortical volume**	
	lh	rh	lh	rh	lh	rh
bankssts	1.65 ± 0.16	1.69 ± 0.13	1.15 ± 0.18	1.21 ± 0.13	1.08 ± 0.17	1.14 ± 0.13
caudalanteriorcingulate	1.38 ± 0.14	1.40 ± 0.14	1.14 ± 0.22	1.19 ± 0.18	1.14 ± 0.24	1.21 ± 0.20
caudalmiddlefrontal	1.77 ± 0.18	1.77 ± 0.19	1.40 ± 0.21	1.31 ± 0.23	1.40 ± 0.22	1.30 ± 0.23
cuneus	1.52 ± 0.19	1.54 ± 0.19	1.34 ± 0.14	1.33 ± 0.14	1.32 ± 0.14	1.28 ± 0.15
entorhinal	1.22 ± 0.23	1.22 ± 0.23	0.82 ± 0.19	0.87 ± 0.18	0.80 ± 0.19	0.81 ± 0.18
fusiform	1.66 ± 0.17	1.71 ± 0.16	1.41 ± 0.18	1.43 ± 0.19	1.33 ± 0.18	1.37 ± 0.20
inferiorparietal	1.81 ± 0.15	1.82 ± 0.13	1.53 ± 0.18	1.59 ± 0.20	1.50 ± 0.17	1.56 ± 0.17
inferiortemporal	1.66 ± 0.17	1.70 ± 0.16	1.37 ± 0.25	1.38 ± 0.21	1.37 ± 0.23	1.41 ± 0.19
isthmuscingulate	1.46 ± 0.12	1.43 ± 0.13	1.27 ± 0.15	1.24 ± 0.15	1.27 ± 0.14	1.27 ± 0.15
lateraloccipital	1.75 ± 0.18	1.77 ± 0.17	1.58 ± 0.15	1.57 ± 0.16	1.49 ± 0.16	1.50 ± 0.15
lateralorbitofrontal	1.65 ± 0.17	1.51 ± 0.15	1.44 ± 0.23	0.95 ± 0.13	1.51 ± 0.16	1.12 ± 0.14
lingual	1.54 ± 0.22	1.52 ± 0.21	1.47 ± 0.18	1.46 ± 0.17	1.50 ± 0.18	1.49 ± 0.18
medialorbitofrontal	1.50 ± 0.15	1.53 ± 0.15	1.09 ± 0.16	1.15 ± 0.14	1.15 ± 0.17	1.21 ± 0.13
middletemporal	1.74 ± 0.16	1.81 ± 0.14	1.42 ± 0.23	1.52 ± 0.19	1.44 ± 0.21	1.55 ± 0.18
parahippocampal	1.54 ± 0.14	1.56 ± 0.12	1.13 ± 0.13	1.09 ± 0.13	1.11 ± 0.13	1.07 ± 0.13
paracentral	1.59 ± 0.22	1.60 ± 0.22	1.40 ± 0.17	1.40 ± 0.19	1.36 ± 0.18	1.36 ± 0.20
parsopercularis	1.74 ± 0.17	1.71 ± 0.16	1.38 ± 0.19	1.30 ± 0.18	1.38 ± 0.19	1.30 ± 0.20
parsorbitalis	1.53 ± 0.20	1.51 ± 0.20	1.21 ± 0.14	1.21 ± 0.18	1.19 ± 0.16	1.22 ± 0.18
parstriangularis	1.68 ± 0.17	1.63 ± 0.19	1.33 ± 0.16	1.30 ± 0.22	1.30 ± 0.16	1.28 ± 0.21
pericalcarine	1.33 ± 0.21	1.30 ± 0.22	1.23 ± 0.20	1.21 ± 0.22	1.18 ± 0.17	1.18 ± 0.17
postcentral	1.84 ± 0.24	1.81 ± 0.26	1.68 ± 0.23	1.69 ± 0.28	1.64 ± 0.20	1.63 ± 0.24
posteriorcingulate	1.57 ± 0.13	1.56 ± 0.14	1.37 ± 0.20	1.35 ± 0.21	1.39 ± 0.19	1.39 ± 0.22
precentral	1.79 ± 0.26	1.76 ± 0.28	1.71 ± 0.24	1.64 ± 0.27	1.72 ± 0.22	1.66 ± 0.28

Continued on next page

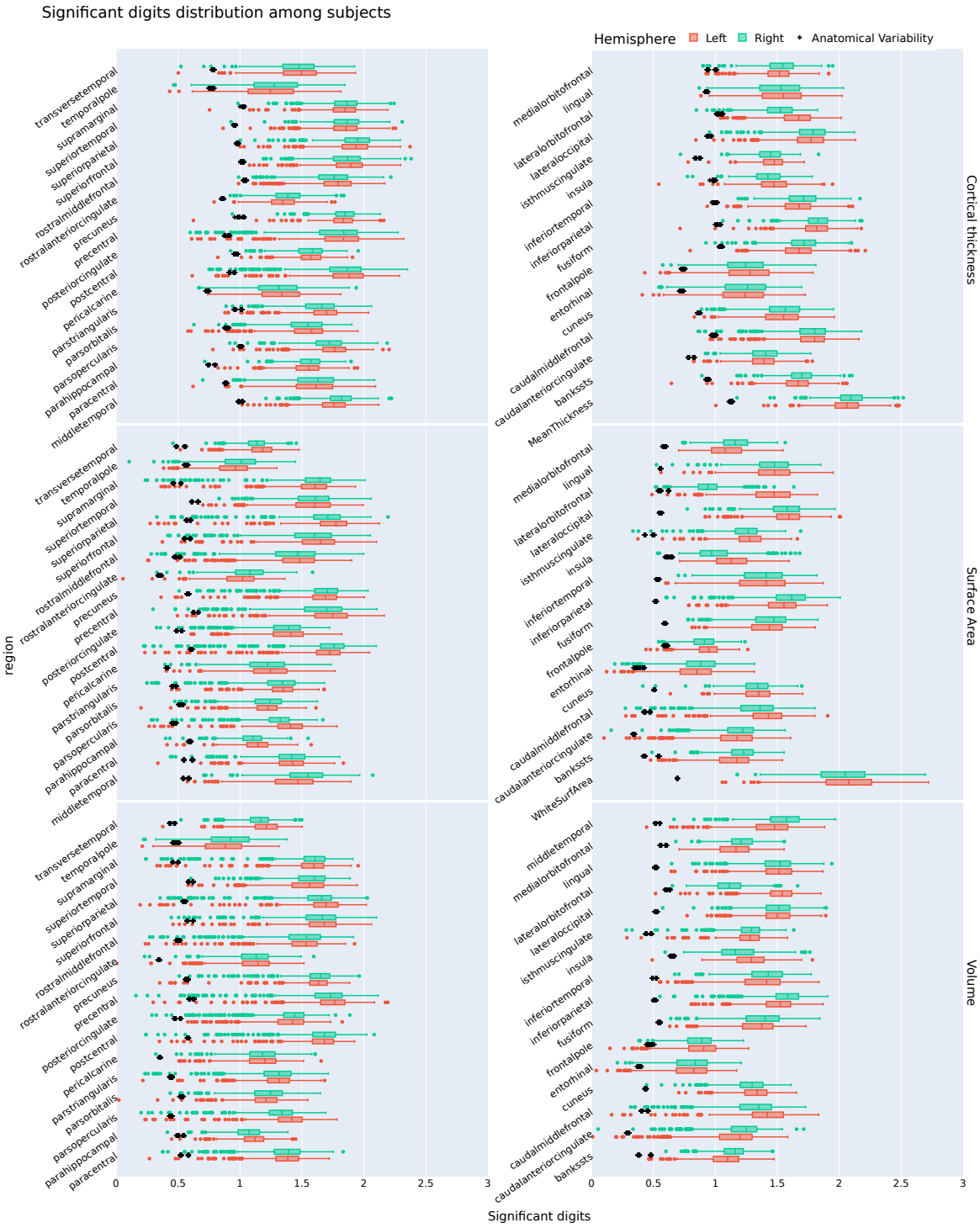

Figure 11: Number of significant digits for each cortical region and metric.

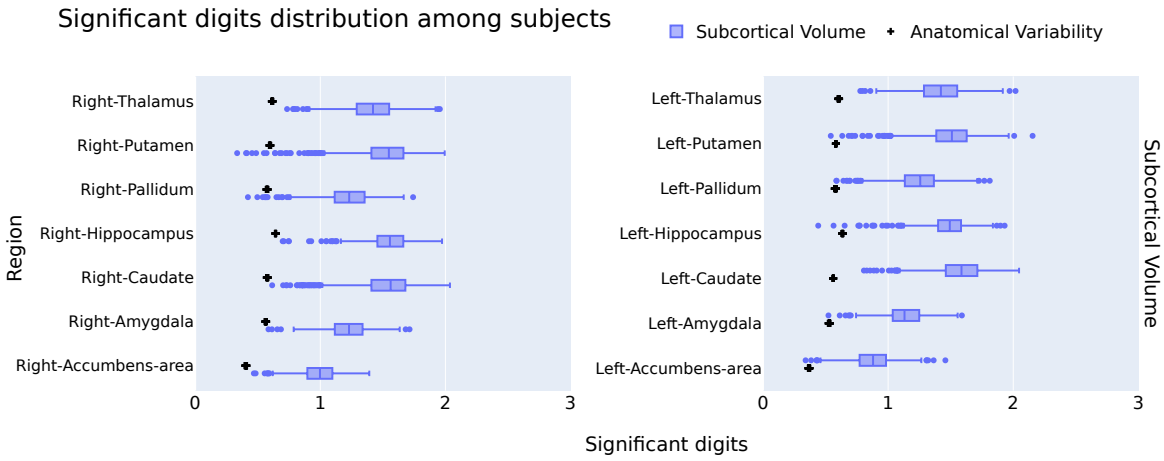

Figure 12: Number of significant digits of subcortical volume for each subcortical region.

Table 2: Significant digits average across all subjects. (Continued)

Region	**cortical thickness**		**surface area**		**cortical volume**	
	lh	rh	lh	rh	lh	rh
precuneus	1.83 ± 0.13	1.84 ± 0.13	1.65 ± 0.21	1.66 ± 0.21	1.61 ± 0.18	1.62 ± 0.19
rostralanteriorcingulate	1.34 ± 0.14	1.39 ± 0.15	1.00 ± 0.16	1.07 ± 0.17	1.11 ± 0.19	1.11 ± 0.18
rostralmiddlefrontal	1.77 ± 0.19	1.74 ± 0.19	1.44 ± 0.24	1.41 ± 0.28	1.49 ± 0.21	1.48 ± 0.25
superiorfrontal	1.87 ± 0.17	1.85 ± 0.18	1.61 ± 0.23	1.56 ± 0.27	1.64 ± 0.21	1.62 ± 0.25
superiorparietal	1.92 ± 0.18	1.93 ± 0.17	1.72 ± 0.24	1.65 ± 0.28	1.66 ± 0.22	1.60 ± 0.26
superiortemporal	1.83 ± 0.17	1.85 ± 0.15	1.57 ± 0.22	1.58 ± 0.18	1.52 ± 0.21	1.57 ± 0.18
supramarginal	1.83 ± 0.16	1.85 ± 0.15	1.57 ± 0.22	1.59 ± 0.26	1.56 ± 0.20	1.56 ± 0.24
frontalpole	1.26 ± 0.23	1.23 ± 0.20	0.94 ± 0.11	0.91 ± 0.11	0.88 ± 0.17	0.87 ± 0.14
temporalpole	1.24 ± 0.26	1.28 ± 0.25	0.94 ± 0.16	0.99 ± 0.19	0.86 ± 0.20	0.91 ± 0.22
transversetemporal	1.47 ± 0.20	1.46 ± 0.18	1.17 ± 0.13	1.13 ± 0.11	1.20 ± 0.15	1.15 ± 0.13
insula	1.47 ± 0.16	1.42 ± 0.14	1.13 ± 0.18	1.00 ± 0.18	1.29 ± 0.16	1.19 ± 0.19

Table 3: Standard-deviation average across all subjects for cortical metrics.

Region	**cortical thickness (mm)**		**surface area (mm^2)**		**cortical volume (mm^3)**	
	lh	rh	lh	rh	lh	rh
bankssts	0.02 ± 0.01	0.02 ± 0.01	28.65 ± 15.97	21.73 ± 8.68	77.25 ± 37.44	59.87 ± 20.45
caudalanteriorcingulate	0.04 ± 0.01	0.04 ± 0.01	19.98 ± 13.83	21.01 ± 14.96	51.33 ± 37.32	51.67 ± 41.74
caudalmiddlefrontal	0.02 ± 0.01	0.02 ± 0.01	38.58 ± 36.77	46.65 ± 44.68	104.41 ± 108.02	124.11 ± 112.10
cuneus	0.02 ± 0.01	0.02 ± 0.01	28.45 ± 11.50	31.25 ± 15.67	60.72 ± 25.52	74.77 ± 34.16
entorhinal	0.08 ± 0.05	0.08 ± 0.05	27.41 ± 16.67	22.37 ± 11.70	125.48 ± 71.07	115.94 ± 57.21
fusiform	0.02 ± 0.01	0.02 ± 0.01	50.70 ± 25.16	47.86 ± 28.19	182.92 ± 92.31	170.22 ± 103.05
inferiorparietal	0.01 ± 0.01	0.01 ± 0.01	53.01 ± 29.19	59.90 ± 50.62	145.66 ± 72.95	159.55 ± 110.14
inferiortemporal	0.02 ± 0.01	0.02 ± 0.01	64.73 ± 42.27	58.75 ± 34.04	198.15 ± 127.44	168.38 ± 84.67
isthmuscingulate	0.03 ± 0.01	0.03 ± 0.01	23.74 ± 11.07	23.35 ± 13.99	57.43 ± 29.59	53.05 ± 34.34
lateraloccipital	0.02 ± 0.01	0.02 ± 0.01	53.82 ± 24.63	56.35 ± 28.61	156.83 ± 66.16	160.98 ± 76.00
lateralorbitofrontal	0.02 ± 0.01	0.03 ± 0.01	43.31 ± 30.16	117.14 ± 33.75	92.60 ± 56.29	217.89 ± 69.06
lingual	0.03 ± 0.01	0.03 ± 0.01	44.26 ± 22.65	46.73 ± 23.96	89.19 ± 46.24	95.82 ± 49.65
medialorbitofrontal	0.03 ± 0.01	0.03 ± 0.01	66.04 ± 24.11	58.06 ± 19.00	147.37 ± 57.84	134.52 ± 42.26
middletemporal	0.02 ± 0.01	0.02 ± 0.01	53.01 ± 34.97	44.87 ± 28.36	165.49 ± 108.52	135.26 ± 77.98

Continued on next page

Table 3: Standard-deviation average across all subjects for cortical metrics. (Continued)

Region	cortical thickness (mm)		surface area (mm^2)		cortical volume (mm^3)	
	lh	rh	lh	rh	lh	rh
parahippocampal	0.03 ± 0.01	0.03 ± 0.01	19.55 ± 8.42	20.45 ± 7.81	64.22 ± 25.29	65.43 ± 24.59
paracentral	0.03 ± 0.02	0.03 ± 0.01	22.94 ± 12.98	26.94 ± 19.80	63.71 ± 40.74	73.88 ± 56.66
parsopercularis	0.02 ± 0.01	0.02 ± 0.01	28.65 ± 28.77	29.46 ± 26.82	80.67 ± 92.87	82.38 ± 89.16
parsorbitalis	0.03 ± 0.02	0.03 ± 0.02	17.82 ± 9.77	21.41 ± 10.66	60.63 ± 45.20	68.18 ± 36.64
parstriangularis	0.02 ± 0.01	0.02 ± 0.01	25.67 ± 14.65	34.86 ± 37.79	71.73 ± 45.49	96.87 ± 102.22
pericalcarine	0.03 ± 0.02	0.04 ± 0.02	36.04 ± 20.18	42.02 ± 24.82	59.64 ± 29.98	68.61 ± 34.89
postcentral	0.01 ± 0.02	0.02 ± 0.02	43.47 ± 67.12	45.98 ± 83.10	100.26 ± 121.35	104.53 ± 156.51
posteriorcingulate	0.02 ± 0.01	0.02 ± 0.01	21.93 ± 13.05	24.39 ± 19.52	52.42 ± 33.33	56.27 ± 52.59
precentral	0.02 ± 0.02	0.02 ± 0.02	46.92 ± 53.54	57.46 ± 70.35	118.04 ± 157.21	148.21 ± 233.10
precuneus	0.01 ± 0.01	0.01 ± 0.00	38.04 ± 42.87	38.95 ± 40.96	100.91 ± 111.15	102.24 ± 96.62
rostralanteriorcingulate	0.05 ± 0.02	0.04 ± 0.02	34.80 ± 15.03	22.00 ± 10.59	81.04 ± 41.59	61.95 ± 33.93
rostralmiddlefrontal	0.02 ± 0.01	0.02 ± 0.01	92.87 ± 96.23	108.40 ± 132.97	213.81 ± 259.58	252.00 ± 358.20
superiorfrontal	0.01 ± 0.01	0.01 ± 0.01	85.23 ± 86.47	98.14 ± 120.75	223.91 ± 234.89	243.75 ± 304.56
superiorparietal	0.01 ± 0.01	0.01 ± 0.01	49.49 ± 80.81	62.89 ± 96.86	132.77 ± 207.97	161.39 ± 235.01
superiortemporal	0.02 ± 0.01	0.01 ± 0.01	47.70 ± 33.64	41.38 ± 23.84	156.30 ± 101.85	129.01 ± 78.70
supramarginal	0.01 ± 0.01	0.01 ± 0.01	50.87 ± 58.82	50.06 ± 83.24	136.23 ± 168.28	133.99 ± 207.69
frontalpole	0.07 ± 0.04	0.07 ± 0.04	12.99 ± 4.02	16.42 ± 4.47	56.49 ± 32.17	67.84 ± 28.93
temporalpole	0.09 ± 0.05	0.08 ± 0.05	25.08 ± 10.71	22.16 ± 11.78	154.60 ± 79.32	138.28 ± 78.33
transversetemporal	0.03 ± 0.02	0.03 ± 0.02	12.73 ± 5.33	9.98 ± 3.33	29.55 ± 12.34	24.91 ± 8.79
insula	0.04 ± 0.02	0.04 ± 0.01	73.45 ± 30.66	95.70 ± 37.63	146.49 ± 64.11	183.39 ± 81.47

Table 4: Significant digits and standard-deviation average across all subjects for subcortical volumes.

Region	Significant digits	Standard deviation (mm^3)
Left-Thalamus	1.42 ± 0.21	120.08 ± 69.61
Left-Caudate	1.57 ± 0.20	38.83 ± 25.11
Left-Putamen	1.49 ± 0.22	65.88 ± 46.39
Left-Pallidum	1.25 ± 0.19	47.81 ± 25.09
Left-Hippocampus	1.48 ± 0.17	56.23 ± 41.03
Left-Amygdala	1.13 ± 0.16	48.71 ± 20.04
Left-Accumbens-area	0.88 ± 0.16	24.20 ± 8.80
Right-Thalamus	1.42 ± 0.20	118.92 ± 68.76
Right-Caudate	1.51 ± 0.24	49.37 ± 42.71
Right-Putamen	1.51 ± 0.25	68.07 ± 70.23
Right-Pallidum	1.22 ± 0.19	49.11 ± 30.50
Right-Hippocampus	1.55 ± 0.18	48.59 ± 28.98
Right-Amygdala	1.23 ± 0.17	42.21 ± 18.68
Right-Accumbens-area	0.99 ± 0.15	20.50 ± 7.72

C Numerical-Anatomical Variability Ratio (ν_{nav})

C.1 ν_{nav} maps

Figures **??** and **??** show the ν_{nav} maps for cortical surface area and volume, respectively. The maps show the average ν_{nav} values across all subjects for each cortical region. The color scale indicates the ν_{nav} value, with warmer colors indicating higher ν_{nav} values. The maps provide a visual representation of the variability in the ν_{nav} values across different cortical regions, highlighting regions with higher

Table 5: Summary of executions failure and excluded subjects. To standardize the sample, we keep 26 repetitions per subject/visits pair. Subject/visit pairs with less than 26 repetitions were excluded which is 12 subjects.

Stage	**Number of rejected repetitions**	**Total number of repetitions**
Cluster failure	1246 (5.80%)	21488
FreeSurfer failure	68 (0.33%)	21488
QC failure	319 (1.48%)	21488
Total	1633 (7.60%)	21488

Status	**Cohort**	**HC**	**PD-non-MCI**	**PD-MCI**
Before QC	n	106	181	29
	Age (y)	60.6 ± 10.2	61.7 ± 9.6	67.7 ± 7.7
	Age range	$30.6 - 84.3$	$36.3 - 83.3$	$49.9 - 80.5$
	Gender (male, %)	58 (54.7%)	119 (65.7%)	–
	Education (y)	16.6 ± 3.3	15.9 ± 2.9	–
After QC	n	103	175	27
	Age (y)	60.7 ± 10.3	61.4 ± 9.5	67.8 ± 7.9
	Age range	$30.6 - 84.3$	$36.3 - 79.9$	$49.9 - 80.5$
	Gender (male, %)	57 (55.3%)	114 (65.1%)	20 (74.1%)
	Education (y)	16.6 ± 3.3	15.9 ± 2.9	15.0 ± 3.5
After MCI exclusion	n	103	121	–
	Age (y)	60.7 ± 10.3	60.7 ± 9.1	–
	Age range	$30.6 - 84.3$	$39.2 - 78.3$	–
	Gender (male, %)	57 (55.3%)	80 (66.1%)	–
	Education (y)	16.6 ± 3.3	16.1 ± 3.0	–
	UPDRS III OFF baseline	–	23.4 ± 10.1	–
	UPDRS III OFF follow-up	–	25.8 ± 11.1	–
	Duration T2 - T1 (y)	1.4 ± 0.5	1.4 ± 0.7	–

Abbreviations: MCI = Mild Cognitive Impairment; UPDRS = Unified Parkinson's Disease Rating Scale; PD = Parkinson's disease. Descriptive statistics before and after quality control (QC). Values are expressed as mean ± standard deviation. PD-non-MCI longitudinal sample is a subsample of the PD-non-MCI original sample that had longitudinal data and disease severity scores available.

or lower ν_{nav} values.

C.2 Consistency results

C.2.1 Consistency of statistical tests

Figures **??** and **??** show the consistency of statistical tests for cortical area and volume, respectively, across all subjects and regions. The plots show the percentage of subjects for which the statistical test was significant ($\alpha = 0.05$) for each region. The consistency varies across regions, with some regions showing higher consistency than others. The red triangles indicate the IEEE-754 run for reference.

C.2.2 Distribution of statistical tests coefficients

Figures **??** and **??** show the distribution of partial correlation coefficients for cortical area and volume, respectively, across all subjects and regions. The red triangles indicate the IEEE-754 run for reference. The distribution shows the variability in the coefficients, with some regions exhibiting higher consistency than others.

C.2.3 Thresholding existing results

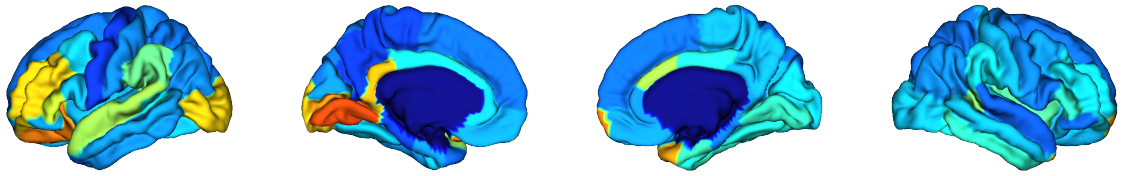

Figure 13: ν_{nav} maps for cortical surface area. The maps show the average ν_{nav} values across all subjects for each cortical region. The color scale indicates the ν_{nav} value, with warmer colors indicating higher ν_{nav} values.

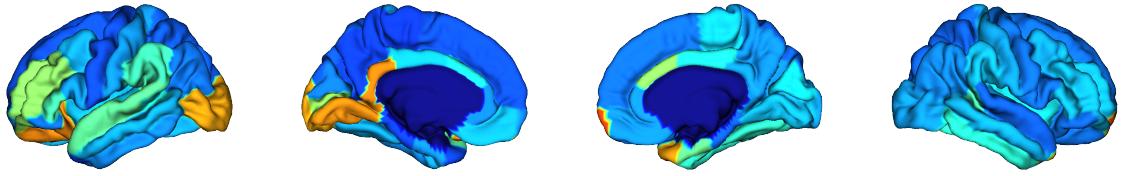

Figure 14: ν_{nav} maps for cortical volume. The maps show the average ν_{nav} values across all subjects for each cortical region. The color scale indicates the ν_{nav} value, with warmer colors indicating higher ν_{nav} values.

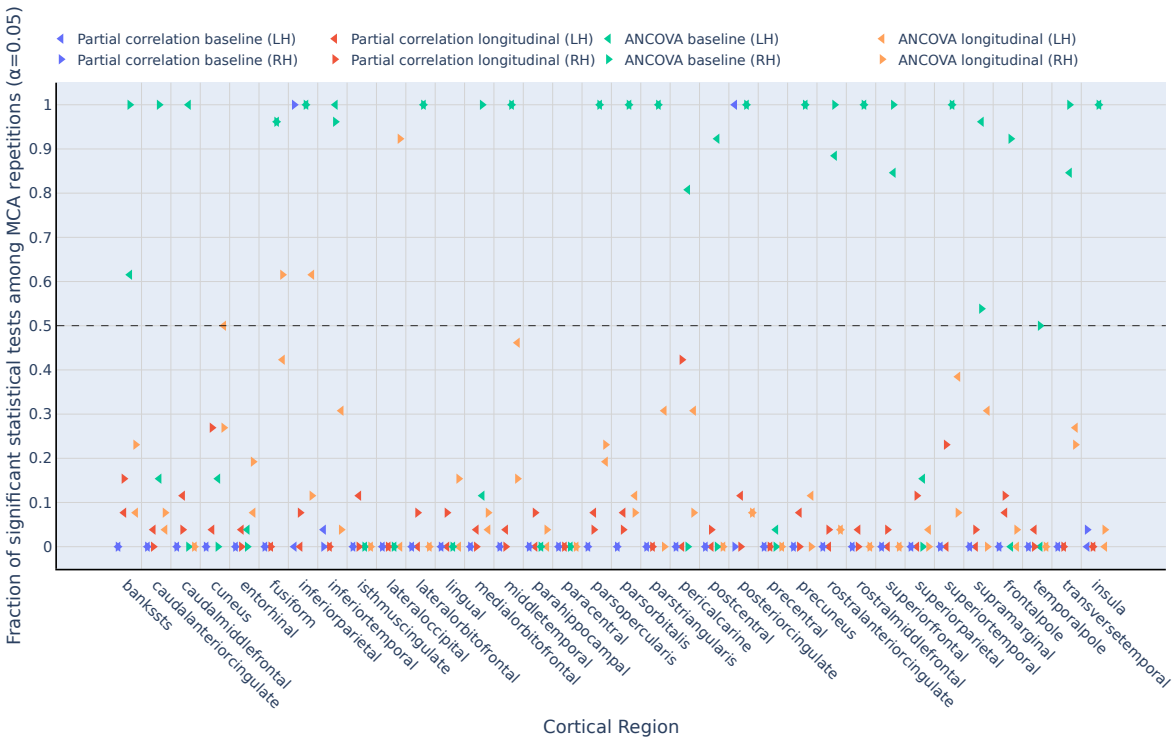

Figure 15: Consistency of statistical tests for cortical area across all subjects and regions. The plot shows the percentage of subjects for which the statistical test was significant ($\alpha = 0.05$) for each region. The consistency varies across regions, with some regions showing higher consistency than others.

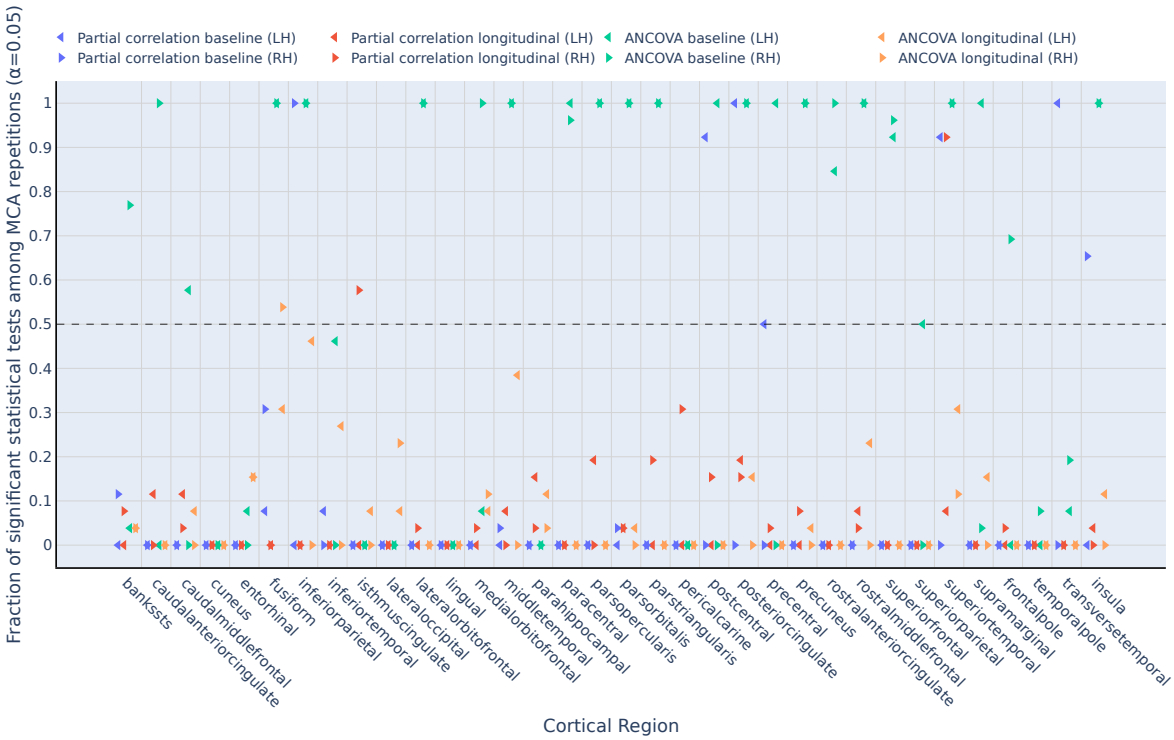

Figure 16: Consistency of statistical tests for cortical volume across all subjects and regions. The plot shows the percentage of subjects for which the statistical test was significant ($\alpha = 0.05$) for each region. The consistency varies across regions, with some regions showing higher consistency than others.

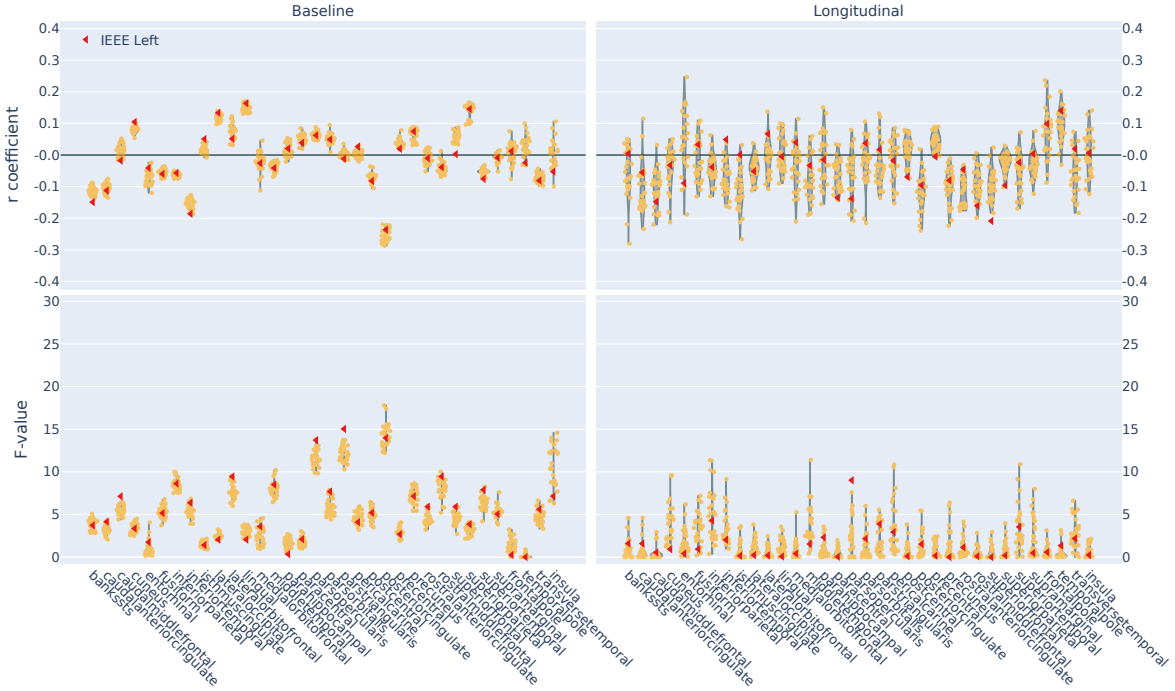

(a) Left hemisphere

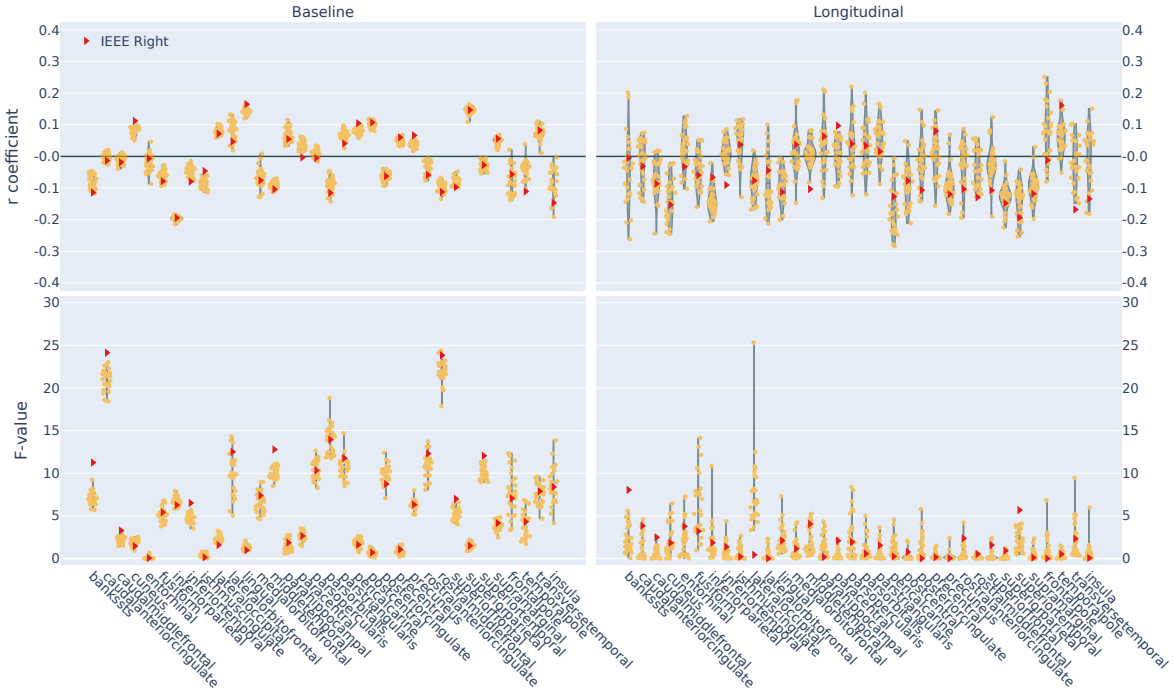

(b) Right hemisphere

Figure 17: Distribution of partial correlation coefficients for cortical area across all subjects and regions. Red triangles indicate the IEEE-754 run for reference. The distribution shows the variability in the coefficients, with some regions exhibiting higher consistency than others.

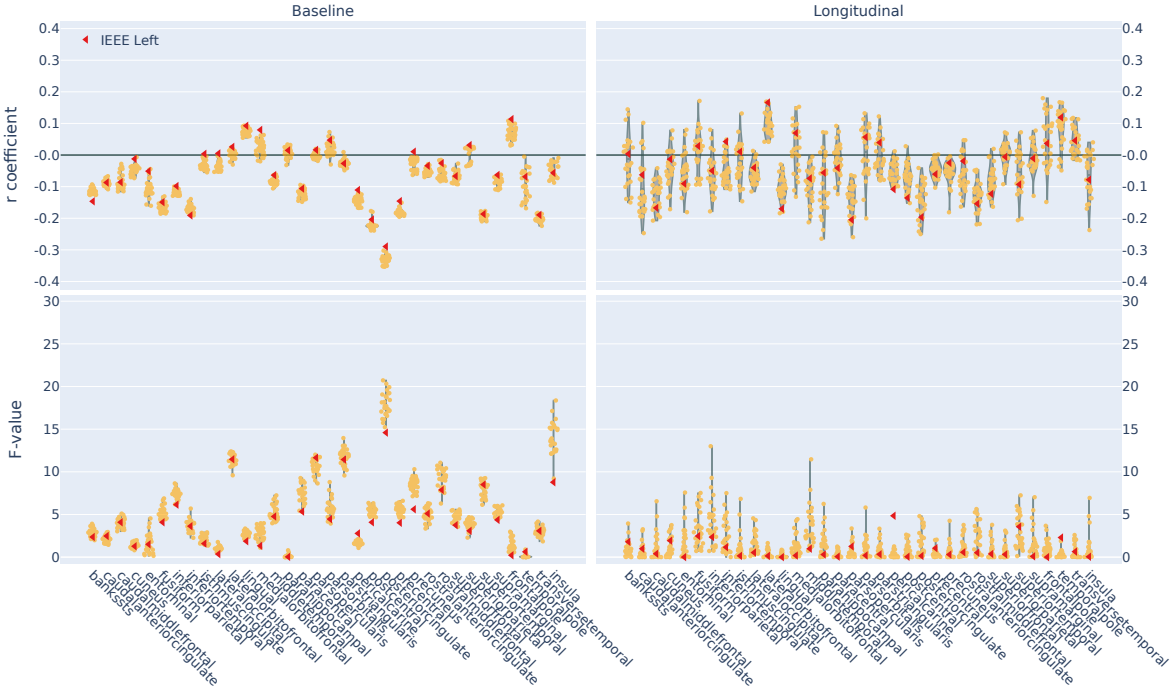

(a) Left hemisphere

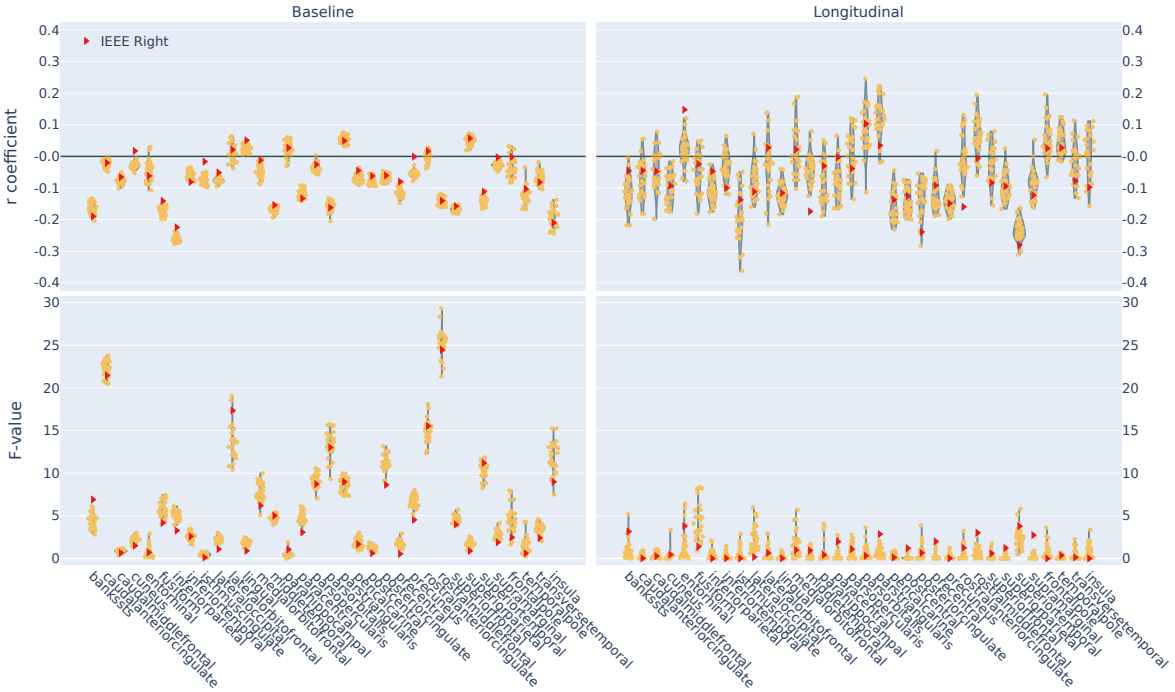

(b) Right hemisphere

Figure 18: Distribution of partial correlation coefficients for cortical volume across all subjects and regions. Red triangles indicate the IEEE-754 run for reference. The distribution shows the variability in the coefficients, with some regions exhibiting higher consistency than others.

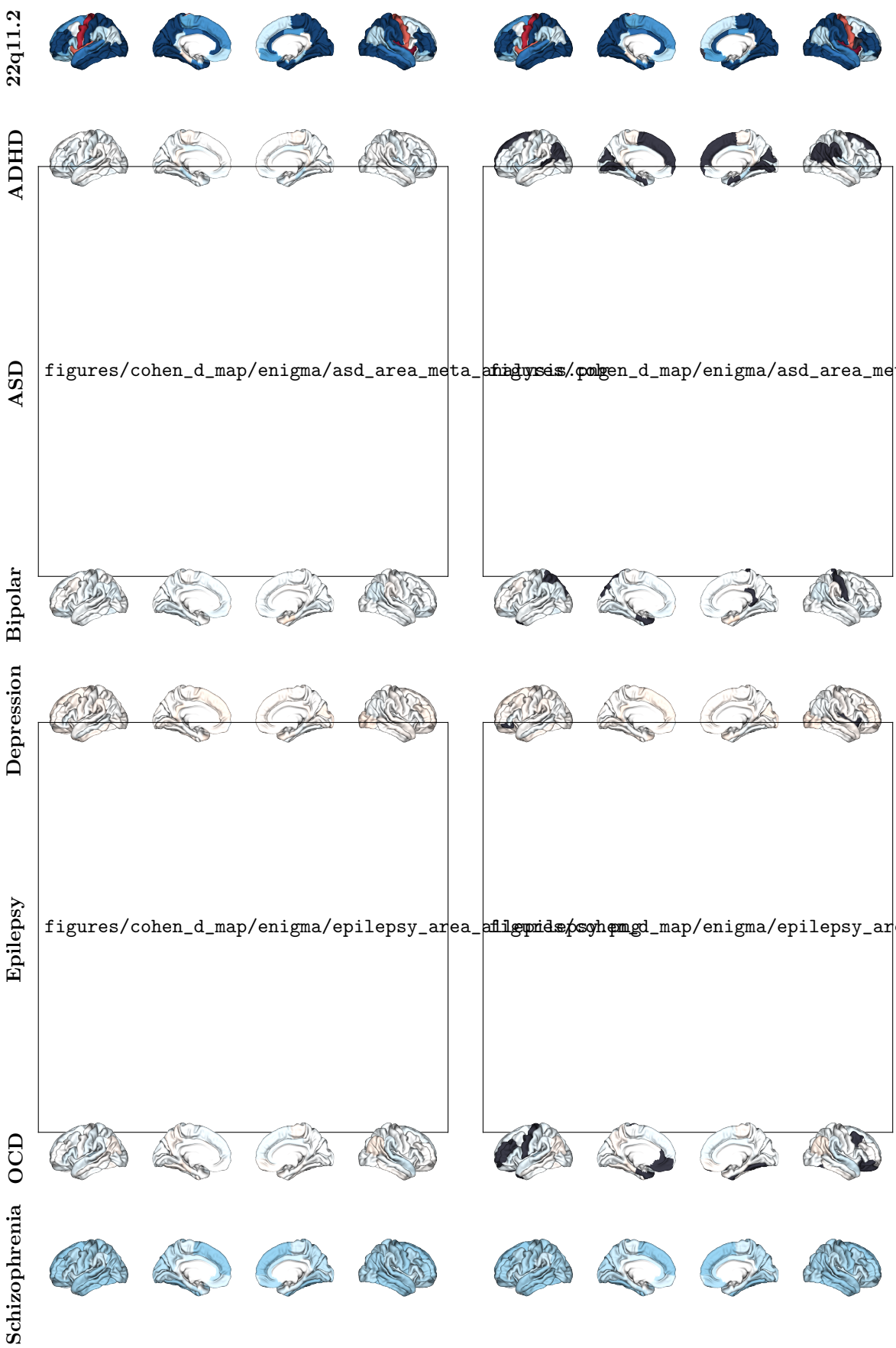

Figure 19: ENIGMA cortical area Cohen's d maps showing unthresholded effect sizes (left) and effect